Biosensors and Bioelectronics 69 (2015) 106–112

Contents lists available at ScienceDirect

Biosensors and Bioelectronics

journal homepage: www.elsevier.com/locate/bios

A novel photoelectrochemical sensor based on photocathode of PbS quantum dots utilizing catalase mimetics of bio-bar-coded platinum nanoparticles/G-quadruplex/hemin for signal amplification

Guang-Li Wang [a,b,*], Kang-Li Liu [a], Jun-Xian Shu [a], Tian-Tian Gu [a], Xiu-Ming Wu [a], Yu-Ming Dong [a], Zai-Jun Li [a]

[a] The Key Laboratory of Food Colloids and Biotechnology, Ministry of Education, School of Chemical and Material Engineering, Jiangnan University, Wuxi 214122, PR China

[b] State Key Laboratory of Analytical Chemistry for Life Science, Nanjing University, Nanjing 210093, PR China

ARTICLE INFO

Article history:
Received 19 November 2014
Received in revised form
15 February 2015
Accepted 16 February 2015
Available online 17 February 2015

Keywords:
Photocathode
PbS quantum dots
Enzyme mimetics
Catalase
Photoelectrochemical biosensor

ABSTRACT

Photocathode based on p-type PbS quantum dots (QDs) combing a novel signal amplification strategy utilizing catalase (CAT) mimetics was designed and utilized for sensitive photoelectrochemical (PEC) detection of DNA. The bio-bar-coded Pt nanoparticles (NPs)/G-quadruplex/hemin exhibited high CAT-like activity following the Michaelis–Menten model for decomposing H_2O_2 to water and oxygen, whose activity even slightly exceeded that of natural CAT. The bio-bar-code as a catalytic label was conjugated onto the surface of PbS QDs modified electrodes through the formed sandwich-type structure due to DNA hybridization. Oxygen in situ generated by the CAT mimetics of the bio-bar-code of Pt NPs/G-quadruplex/hemin acted as an efficient electron acceptor of illuminated PbS QDs, promoting charge separation and enhancing cathodic photocurrent. Under optimal conditions, the developed PEC biosensor for target DNA exhibited a dynamic range of 0.2 pmol/L to 1.0 nmol/L with a low detection limit of 0.08 pmol/L. The high sensitivity of the method was resulted from the sensitive response of PbS QDs to oxygen and the highly efficient CAT-like catalytic activity of the bio-bar-coded Pt NPs/G-quadruplex/hemin.

1. Introduction

Photoelectrochemical (PEC) analysis is a newly emerging and dynamically developing analytical method. It has the merits of simple equipment, cost-effectiveness, suitableness for miniaturization, high sensitivity and rapidness for detection (Wang et al., 2009a, 2009b; Zhao et al., 2014). The photoelectrochemically active materials largely determine the performance of the PEC sensors because the PEC detection is based on the interaction between the excited photoelectrochemically active materials and the analytes (Wang et al., 2010; Shi et al., 2011). The extensively studied PEC sensors based on photoanodes made by n-type semiconductors (such as sensitized TiO_2 or CdS quantum dots (QDs)) showed sensitive response to a variety of reductive substances, such as ascorbic acid (Wang et al., 2009a, 2009b), H_2O_2 (An et al., 2010; Tu et al., 2012; P.P. Wang et al., 2013), nicotinamide adenine dinucleotide (NADH) (Schubert et al., 2010), and thio compounds (Long et al., 2011; Zhao et al., 2012). This was because the photogenerated holes of n-type semiconductors would transfer to their surface and react with the reductive substances (acting as electron donors). However, these PEC sensors based on photoanodes are obsessed by a relatively poor selectivity in biological samples because many reductive agents coexist in biological fluids (Zachariou and Hearn, 2000; Qian et al., 2012; Kaya and Volkan, 2012; Beitollahi et al., 2008; Mazloum-Ardakani et al., 2011, 2012). Luckily, we recently found that photocathode made by CdS QDs sensitized p-type nickel oxide hardly showed any response to reductive species (Wang et al., 2014), indicating its improved selectivity for biosensing. For p-type semiconductors, photogenerated electrons immigrate to their surface (Choudhary et al., 2012), leading to their preferable interaction with electron acceptors but not electron donors in the electrolyte solution. It seems that the exploration of photocathode in PEC analysis would broaden the scope of photoelectrochemistry in biosensing. However, at present, the PEC detection platforms based on photocathodes are still very limited (Wang et al., 2014).

As a narrow band gap (bulk: 0.41 eV at 300 K) semiconductor,

* Corresponding author at: The Key Laboratory of Food Colloids and Biotechnology, Ministry of Education, School of Chemical and Material Engineering, Jiangnan University, Wuxi 214122, PR China.
E-mail address: glwang@jiangnan.edu.cn (G.-L. Wang).

http://dx.doi.org/10.1016/j.bios.2015.02.027
0956-5663/

PbS is of particular interest because of its large exciton Bohr radius (Jankovič et al., 2010; Scholes and Rumbles, 2006; Seghaier et al., 2006), easily tuned electronic property (Kang et al., 2011) and the multiple exciton effect (Sukhovatkin et al., 2009; Sambur et al., 2010; Rabani and Baer, 2010). In addition, different from the commonly used n-type CdS QDs, PbS usually demonstrates p-type conductivity (García-Valenzuela et al., 2013). Though with these intriguing characteristics, PbS QDs have never been exploited in PEC analysis.

Enzyme-mediated signal amplification methodologies (by employing enzymes or enzyme mimetics as amplification labels) have attracted great attention for highly sensitive determination of target biomolecules. Natural enzymes including horseradish peroxidase (HRP) and alkaline phosphatase (ALP) have been widely applied in biosensors due to their unique merits: highly catalytic activity, high specificity, mild reaction conditions, and easy conjugation to biomolecules and nanomaterials (Perfezou et al., 2012). Though great successes have been made by HRP or ALP in biosensing, to develop other innovative and powerful labels based on enzymes or enzyme mimetics to achieve signal amplification is still a hot spot. Catalase (CAT) has shown great potentials in biosensing because it is more efficient and much cheaper than other popular alternatives such as HRP and ALP (Yu and Caruso, 2003; Roberto and Stevens, 2012; Zhang et al., 2013). The most prominent characteristics of CAT is its ultrahigh catalytic property, which can catalyze the decomposition of millions of hydrogen peroxide (H_2O_2) to water and oxygen in one second (Ammam and Fransaer, 2011). CAT is promising as a biocatalytic label for the construction of novel biosensors (Gao et al., 2013).

Compared to natural enzymes, artificial enzymes have several superiority (Gao et al., 2007; Xie et al., 2012; Wei and Wang, 2013). For example, G-quadruplex/hemin is a novel catalytic nucleic acid (DNAzyme) formed by hemin intercalated in guanine-rich nucleic acid sequences (Travascio et al., 2001), which possesses several unique features, such as it is less expensive to produce, relatively facile for labeling, and more resistant to hydrolysis and heat treatment (Yuan et al., 2012).

Considering the advantages of photocathode, CAT and enzyme mimetics, our motivation is to combine the ultrahigh catalytic activity of CAT mimetics with the merits of photocathode to exploit a novel PEC detection platform for DNA. Different from the commonly used peroxidase-like activity of the G-quadruplex/hemin (Deng et al., 2008; Li et al., 2011; Shimron et al., 2012), herein, we found that it demonstrated CAT-like activity for catalyzing the decomposition of H_2O_2 to water and oxygen. By combining the G-quadruplex/hemin with platinum nanoparticles (Pt NPs) (Fan et al., 2011; X.Y. Wang et al., 2013), a highly efficient CAT mimetics of bio-bar-coded Pt NPs/G-quadruplex/hemin was formed. The CAT mimetics of the bio-bar-code as an amplifying label catalyzed the decomposition of H_2O_2 to generate an efficient electron acceptor of PbS QDs–oxygen, leading to obviously magnified photocurrent of PbS QDs. This "switch-on" PEC sensor based on PbS QDs and CAT mimetics of the bio-bar-code was highly sensitive and selective for the detection of the target DNA. The methodology not only exploited the PbS QDs based photocathode in PEC sensing but also provided a powerful PEC tool based on CAT mimetics for biosensors.

2. Experimental details

2.1. Chemicals, materials and instrumentation

$Pb(NO_3)_2$, thioglycolic acid (TGA), hemin, $NaBH_4$ (96 wt%), H_2O_2 (30 wt%), $H_2PtCl_6 \cdot 6H_2O$, *N*-hydroxysuccinimide (NHS), tris(2-carboxyethyl) phosphine hydrochloride (TCEP), $K_4Fe(CN)_6 \cdot 3H_2O$, $K_3Fe(CN)_6$ were purchased from Sinopharm Chemical Reagent Co., Ltd. (Shanghai, China). $Na_2S \cdot 9H_2O$ was purchased from Shanghai TongYa Chemical Reagent Co., Ltd. (Shanghai, China). Catalase, 1-ethyl-3-(3-dimethylaminepropyl) carbodiimide (EDC) and poly (diallyldimethylammonium chloride) (PDDA, 20%, w/w in water, molecular weight=200,000–350,000) were obtained from Sigma-Aldrich (St. Louis, USA). Indium tin oxide (ITO) glass was purchased from Southern Glass Holding Co., Ltd. (type N-STN-S1-10, ITO coating 180 ± 20 nm, sheet resistance 8.1 ± 0.6 Ω/sq., Shenzhen, China). All the synthetic oligonucleotides, which were used as models of the developed DNA sensor, were purchased from Sangon Biotechnology Co., Ltd. (Shanghai, China). The sequences of the capture probe, reporter probe, target DNA, and non-complementary DNA is listed as follows:

Capture probe: 3′-NH_2-$(CH_2)_6$-T CGC ATC CTA TCT-5′;
Reporter probe: 3′-A TAT GCC AAG CGC GGG GTA GGG CGG GTT GGG TTT-$(CH_2)_6$-SH-5′;
Target DNA: 5′-AGC GTA GGA TAG ATA TAC GGT TCG CGC-3′.

Non-complementary DNA (nonspecific control 1 and nonspecific control 2) with three or seven mismatched bases indicated in italics with underline: 5′-AGC GTA GGA TAG A*AA* *AAG* GGT TCG CGC-3′ (nonspecific control 1) and 5′-AGC GTA GGA TAG ATA *GG*C GG*G AT*G *GGT*-3′ (nonspecific control 1).

PEC measurements were performed with a homemade system utilizing a 500 W Xe lamp (NBeT, China) equipped with an ultraviolet cutoff filter ($\lambda \geq 400$ nm) as irradiation source and a CHI 800C electrochemical workstation (Shanghai Chenhua, China) for photocurrent measurements. PbS QDs modified ITO electrode with an area of 0.25 cm^2, a Pt wire and a saturated Ag/AgCl was employed as the working, counter and reference electrode, respectively. The photocurrent measurements were performed at a constant potential of 0 V (vs saturated Ag/AgCl) in 0.1 mol/L Tris–HCl (pH 7.0) as the supporting electrolyte. High resolution transmission electron microscopy (HRTEM) images were acquired on a JEOL JEM-2100 transmission electron microscope (Hitachi, Japan). The X-ray powder diffraction (XRD) was obtained using an X'Pert Philips materials research diffractometer (D8, Brook AXS, Germany) employing a scanning speed of $0.02^\circ\ s^{-1}$. UV–vis–NIR absorption spectroscopic measurements were carried out using a Shimadzu UV–vis–NIR-3600 spectrophotometer (Shimadzu, Japan). Gas detections were carried out using a GC9790 gas chromatograph (Zhejiang Fuli Analytical Instrument Co. Ltd., China). Electrochemical impedance spectroscopy (EIS) was carried out on a CHI 660D electrochemical workstation (Shanghai Chenhua, China) in 0.1 M KCl containing a redox probe of 5.0 mM $K_3[Fe(CN)_6]/K_4[Fe(CN)_6]$ (1:1) mixture with an applied voltage of 5 mV over a frequency range of 2–900 kHz. A 15% native polyacrylamide gel electrophoresis (PAGE) was prepared by using 1 × Tris-borate–EDTA (TBE) buffer. 7 μL of DNA sample was mixed with 2 μL of native loading buffer (10 ×) and loaded into 15% native polyacrylamide gel. The gel electrophoresis was run at 100 V for 120 min in 1 × TBE buffer. After that, gel was stained with ethidium bromide (EB) for 30 min. The resulting board was illuminated with UV light and photographed with a Molecular Imager Gel Doc XR (Bio-Rad, USA).

2.2. Synthesis of PbS QDs and fabrication of PbS QDs modified ITO (ITO/PbS) electrodes

Thioglycolic acid (TGA)-capped PbS QDs were synthesized according to a slightly modified procedure (Yu et al., 2012). The synthetic details and the fabrication of PbS QDs modified ITO (ITO/PbS) electrodes are shown in the supplemental information.

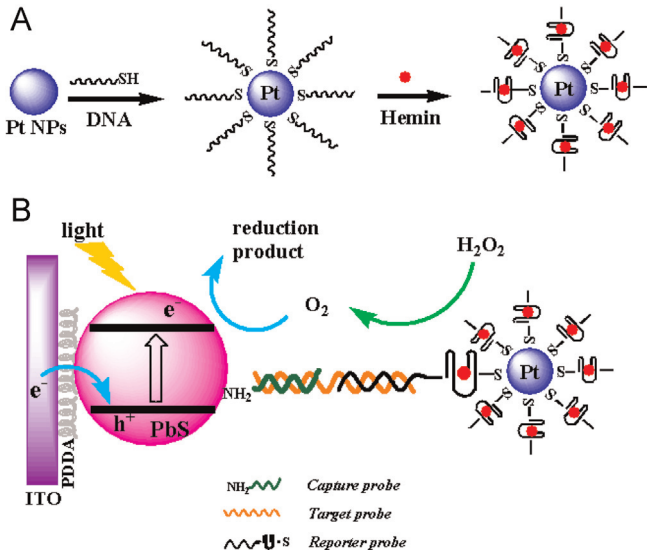

Scheme 1. (A) Schematic representation of the preparation procedure for the bio-bar-coded Pt NPs/G-quadruplex/hemin. (B) The detection mechanism of the PEC DNA sensor.

2.3. Preparation of PDDA-capped Pt NPs

PDDA-capped Pt NPs were synthesized using a slightly modified procedure reported by Zhang et al. (2009). See Supplementary information for the detailed synthesis procedure.

2.4. Fabrication of bio-bar-coded Pt NPs/G-quadruplex/hemin

The fabrication of bio-bar-coded Pt NPs/G-quadruplex/hemin is shown in Scheme 1A. The as-synthesized Pt NPs was connected to the activated thiol group of the reporter probe (5′-SH-C_6-ssDNA). The reporter probe is consisted of two domains: one domain has a lot of G bases, which is able to form G-quadruplex and embed hemin to form G-quadruplex/hemin; the other domain can hybrid with the target DNA. The details for the synthesis of the bio-bar-coded Pt NPs/G-quadruplex/hemin are provided in Supplementary information.

2.5. Investigation of the CAT-like activity of the bio-bar-coded Pt NPs/G-quadruplex/hemin

A series of H_2O_2 solutions with different concentrations were prepared with 0.1 mol/L Tris–HCl (pH 7.0) buffer solution. 10 μL of the as-synthesized bio-bar-coded Pt NPs/G-quadruplex/hemin or 10 μL of CAT was mixed with H_2O_2 solutions with different concentrations. The reactions were monitored at 240 nm characteristic of H_2O_2 absorption using a UV–vis spectrophotometer. The concentration of H_2O_2 can be calculated by Lambert–Beer law ($A_{240}=\varepsilon bc$), where c is the concentration of H_2O_2, A_{240} is the absorbance of the reaction solution at 240 nm, and ε is the molar absorption coefficient of H_2O_2 at 240 nm (43.6 L mol^{-1} cm^{-1}) (X. Y. Wang et al., 2013).

2.6. PEC detection of DNA

The immobilization of capture probe onto the electrodes modified by PbS QDs was achieved by using the classic EDC/NHS coupling reactions between –COOH groups of the TGA-capped PbS QDs and the –NH_2 groups of capture probe. The PbS QDs modified electrodes were immersed in an aqueous solution containing 10 mg/mL EDC and 5 mg/mL NHS for 1 h at room temperature and were subsequently rinsed with 10 mM Tris–HCl (pH 7.4, C_{NaCl}=0.1 mol/L) carefully. Then, 20 μL of capture probe (1 μM) in 10 mM Tris–HCl (pH 7.4, C_{NaCl}=0.1 mol/L) was dropped onto the surface of the electrodes and incubated at 4 °C overnight, followed by blocking with 0.01 mol/L Tris–HCl (pH 7.4, C_{NaCl}=0.1 mol/L) containing 1.0 mmol/L monoethanolamine (MEA) and washing with 10 mM Tris–HCl (pH 7.4, C_{NaCl}=0.1 mol/L). The obtained electrodes were designated as ITO/PbS/capture. The ITO/PbS/capture electrode was then put into a sealed PEC cell and immersed in 2 mL of 0.1 mol/L Tris–HCl (pH 7.0, C_{NaCl}=0.1 mol/L, C_{KCl}=0.05 mol/L). High pure nitrogen was bubbled for 30 min throughout the electrolyte to remove dissolved oxygen and the photocurrent of the ITO/PbS/capture electrode was measured (defined as I_0).

Certain concentration of target DNA (20 μL) and bio-bar-coded Pt NPs/G-quadruplex/hemin complex was spread on the ITO/PbS/capture electrode and incubated for 1 h at 37 °C in 10 mM Tris–HCl (pH 7.4, 0.1 mol/L NaCl and 0.05 mol/L KCl) followed by washing. Therefore, the sandwich DNA structure was assembled on the electrode. After bubbling the supporting electrolyte solution (0.1 mol/L Tris–HCl, pH 7.0, C_{NaCl}=0.1 mol/L, C_{KCl}=0.05 mol/L) with high pure nitrogen for 30 min, certain concentration of H_2O_2 was injected rapidly and the photocurrent (defined as I) was recorded 2 min later.

3. Results and discussion

3.1. Morphology and composition characterization

Sharp diffraction peaks appeared at scattering angles (2θ) of 25.94°, 30.02°, 43.02°, 50.86°, 53.44°, 62.38°, 68.80°, 71.02° and 78.84° in the X-ray diffraction (XRD) pattern of the PbS QDs (Fig. 1). All these peaks corresponded to scattering from the (111), (200), (220), (311), (222), (400), (331), (420) and (422) planes of the standard cubic PbS [JCPDS file no. 5-592], demonstrating that the product was face-centered cubic PbS. The TEM image of the as-synthesized PbS QDs confirmed its spherical morphology with diameters of about 6–8 nm (Fig. S1A). The inset HRTEM image of individual ultrasmall PbS QDs revealed the clear lattice spacing of ~0.17 nm, corresponding to the (222) plane of the cubic structure of PbS. The as synthesized PDDA-capped Pt NPs were with sizes of about 2–5 nm (Fig. S1B).

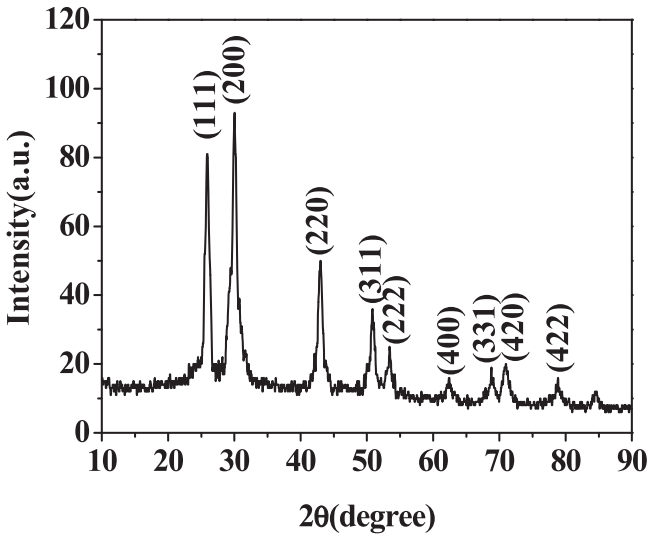

Fig. 1. XRD pattern of PbS QDs.

3.2. The CAT-like catalytic activity of bio-bar-coded Pt NPs/G-quadruplex/hemin

As one of the most important antioxidant enzymes in organisms, CAT, is consisted of four heme groups. It can quickly catalyze the decomposition of millions of H_2O_2 molecules into water and oxygen per second (Nelson and Kiesow, 1972). In our experiment, the characteristic absorption of H_2O_2 at 240 nm (X.Y. Wang et al., 2013) in the presence of Pt NPs or G-quadruplex/hemin (hemin embedded into the G-quadruplex) decreased (Table S1) with the simultaneous generation of oxygen bubbles (Fig. S2) as proved by gas chromatography. Therefore, both of the as-synthesized Pt NPs and G-quadruplex/hemin had CAT-like activity. By combining Pt NPs and the reporter probe to form a bio-bar-coded Pt NPs/G-quadruplex/hemin, a more efficient CAT mimetics than that of Pt NPs or G-quadruplex/hemin alone formed (Fig. S2 and Table S1). The enhanced catalytic activity of the bio-bar-code was resulted from the cooperative effect of Pt NPs and G-quadruplex/hemin. Similar to natural enzymes, the relative catalytic activities of the bio-bar-coded Pt NPs/G-quadruplex/hemin for the decomposition of H_2O_2 were also influenced by solution pH and temperature (Fig. S3). The catalytic activity of CAT decreased obviously when the solution pH increased from 6.0 to 9.0 due to the cleavage of disulfide bonds in the protein structure in alkaline solutions (Messens and Collet, 2006). For natural CAT, subtle change in its structure or conformation will lead to significant decrease or even loss of its catalytic activity (X.Y. Wang et al., 2013). The optimum pH for the catalytic activity of the bio-bar-code was 7.0. A decrease in the catalytic activity was observed at solutions with higher or lower pH than 7.0. From Fig. S3B we can know that the catalytic activity of the bio-bar-code increased continuously with the elevated temperature from 5 to 90 °C. While CAT reached its maximum catalytic activity around 37 °C and showed markedly decrease in catalytic activity at higher temperatures. It should be pointed out that the bio-bar-code showed improved stability compared to CAT at higher temperatures, indicating its better stability under harsh conditions.

Under a certain concentration range of H_2O_2, the catalytic behaviors of CAT and bio-bar-coded Pt NPs/G-quadruplex/hemin for H_2O_2 decomposition followed the Michaelis–Menten kinetic model (Fig. 2). According to the Lineweaver–Burk double reciprocal curve $1/\upsilon = K_m/\upsilon_{max}\cdot 1/[S] + 1/\upsilon_{max}$ (υ represents the total reaction rate, K_m represents the Michaelis constant, υ_{max} represents the maximum reaction rate, [S] is the concentration of substrate) (Mu et al., 2012), the K_m value of the bio-bar-coded Pt NPs/G-quadruplex/hemin complex was 24.9 mM. This K_m value was a little lower than that of CAT (28.7 mM), indicating that the bio-bar-code had a slightly better affinity for the substrate of H_2O_2. This higher affinity was due to the cooperative effect of Pt NPs and G-quadruplex/hemin in the bio-bar-code with more "active sites", while CAT only had one catalytic center. Furthermore, the K_m value of the bio-bar-code was also much lower than that (126.1 mM) of the CAT mimetics based on polyamidoamine dendrimer encapsulated Pt NPs (X.Y. Wang et al., 2013).

3.3. PEC response of the ITO/PbS electrode

The UV–vis–NIR absorption spectrum implied that the PbS QDs had a broad absorption range from 400 to 1300 nm (Fig. S4), implying that they were suitable for the employment as photoactive materials under the light ($\lambda \geq 400$ nm) irradiation. The ITO/PbS QDs electrode showed cathodic photocurrent under irradiation in air-saturated Tris–HCl solution (pH 7.0) (Fig. 3). It should be reasonable to observe cathodic photocurrent for PbS QDs since it is usually a p-type semiconductor (Acharya and Bose, 1971; García-Valenzuela et al., 2013). As a p-type semiconductor, electrons transfer faster towards the electrolyte than that of holes with the simultaneous hole-capture by the electrons from the ITO

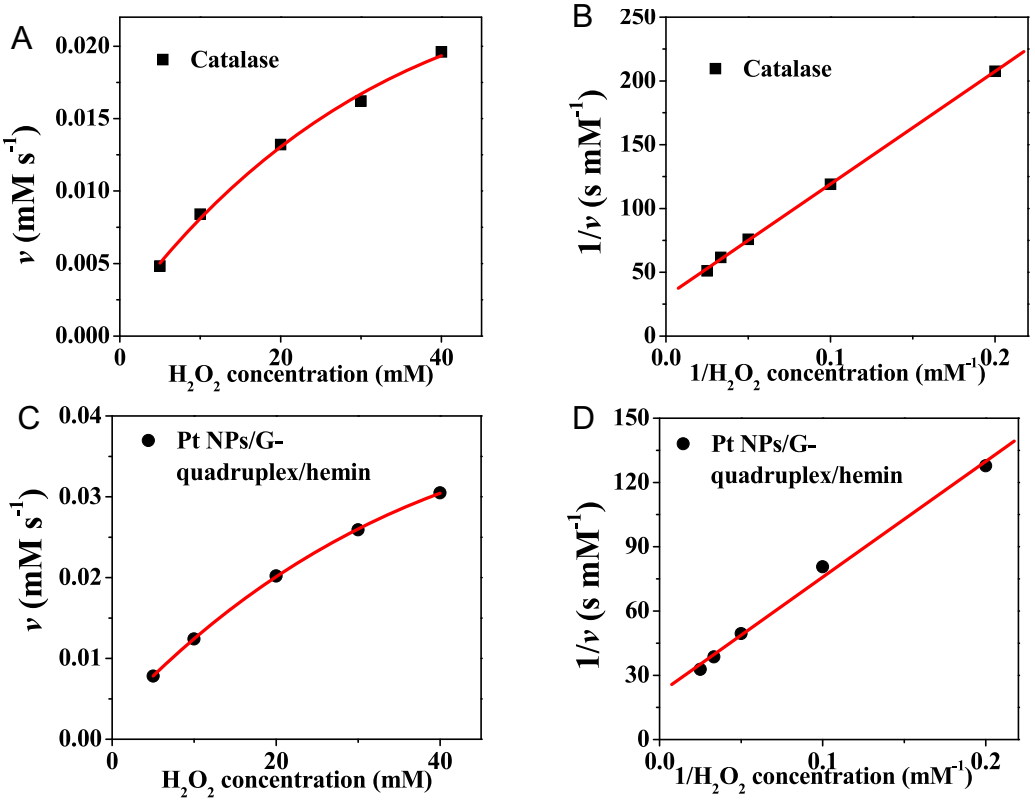

Fig. 2. Michaelis–Menten curve (A, C) and double reciprocal curve (B, D) of CAT (A, B) and the bio-bar-coded Pt NPs/G-quadruplex/hemin (C, D).

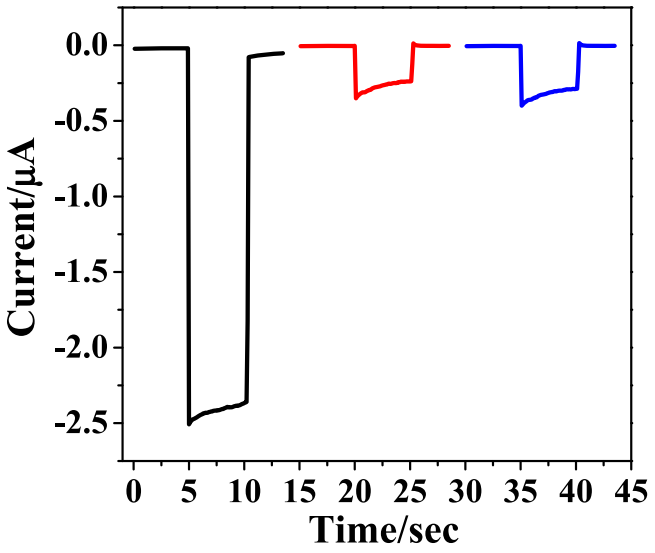

Fig. 3. Photocurrent of the PbS QDs in aerated (black line) or deaerated Tris–HCl solution (pH 7.0) before (red line) and after (blue line) the addition of 2.0×10^{-4} mol/L H_2O_2. (For interpretation of the references to color in this figure legend, the reader is referred to the web version of this article.)

electrode, leading to the flow of cathodic photocurrent (Acharya and Bose, 1971; Choudhary et al., 2012). Also, it was found that the cathodic photocurrents of ITO/PbS electrodes increased with increased cathodic potentials (Fig. S7), which also indicated the p-type conductivity nature of the PbS QDs (Hu et al., 2008).The cathodic photocurrent of the PbS QDs was greatly suppressed (by 90.1%) after bubbling the solution with high pure nitrogen. This phenomenon could be explained by the fact that the dissolved oxygen in the aerated solutions could act as an electron acceptor to scavenge the photogenerated electrons of the illuminated PbS QDs, thus enhancing charge separation and greatly magnifying cathodic photocurrent. As is known, the cathodic photocurrent of the p-type semiconductors can be largely promoted by a suitable electron acceptor in the supporting electrolyte (Powar et al., 2013; Wang et al., 2014).

In order to confirm the photoinduced electron transfer (PET) between illuminated PbS QDs and oxygen, electrochemical methods were employed to study the conduction band (CB) and valence band (VB) edge of PbS QDs (Yeh et al., 2013). Results showed that PbS had a CB edge at −0.83 eV and a VB edge at 0.34 eV vs Ag/AgCl (saturated KCl) (Fig. S5). That is, the CB and VB potential of PbS QDs was −0.63 and 0.54 V vs normal hydrogen electrode (NHE), respectively. The CB (−0.63 V vs NHE) of PbS QDs was more negative than the reduction potential of oxygen (0.815 V vs NHE). As a result, oxygen could act as an electron acceptor of the illuminated PbS QDs.

The electrolyte solution pH and applied potential influenced the interaction between the ITO/PbS photocathode and oxygen (Fig. S6A). The photocurrent responses ($(I-I_0)/I_0$, where I_0 and I were the photocurrents of ITO/PbS electrodes in the absence and presence of dissolved oxygen, respectively) approached its maximum when the pH of Tris–HCl buffer solution was 7.0 and the applied potential was 0 V.

3.4. PEC detection of DNA

Based on the fact that the cathodic photocurrent of PbS QDs was sensitive to dissolved oxygen and was unaffected by H_2O_2 (Fig. 3), a novel PEC DNA sensor was developed employing the bio-bar-coded Pt NPs/G-quadruplex/hemin complex with efficient CAT-like catalytic activity to decompose of H_2O_2 to release oxygen for signal amplification (shown in Scheme 1B). The capture probe covalently immobilized on PbS QDs hybridized with one end of the target DNA and then the other end of the target DNA hybridized with the bio-bar-coded Pt NPs/G-quadruplex/hemin, forming a sandwich structure. The bio-bar-coded Pt NPs/G-quadruplex/hemin with CAT-like activity catalyzed the decomposition of H_2O_2 to release oxygen, and oxygen acted as an electron acceptor to promote the generation of enhanced cathodic photocurrent of PbS QDs.

Electrochemical impedance spectroscopy (EIS) and cyclic voltammetry (CV) were adopted to characterize the assembly process of the DNA sensor. The impedance spectrum includes a semicircle portion and a linear portion, which represent the electron-transfer and the diffusion limited process respectively. The value of the diameter of the semicircle reflects the interfacial electron-transfer resistance (R_{et}) (Lu and Hu, 2006). As shown in Fig. S8A, the bare ITO electrode with good conductivity exhibited a small semicircle (curve a). After the assembly of TGA-capped PbS QDs, the surface turned to be negatively charged, which obstructed the access of the $Fe(CN)_6^{3-/4-}$ molecules to the electrode surface, resulting in the remarkably increase of the R_{et} for ITO/PbS (curve b). After the capture probe was immobilized to the electrode surface by the covalent reaction, the R_{et} of ITO/PbS/capture further increased (curve c), which was attributed to the poor conductivity of single strand DNA and the phosphate backbone of DNA with negative charge. After further hybridization to target DNA, the R_{et} of ITO/PbS/capture/target increased again (curve d). This was because the negative charge of the formed double-strand DNA was more than that of single strand DNA (Patolsky et al., 2002). The R_{et} change resulted from the nonspecific DNA (nonspecific control 1 and nonspecific control 2) was much smaller than that from the target DNA, confirming that the hybridization was specific for the target. The final R_{et} increased and showed the largest value after incubating the electrode with the bio-bar-coded Pt NPs/G-quadruplex/hemin (curve e). The main reasons were the steric effect of double-strand DNA with increased negative charge density and the bio-bar-coded Pt NPs/G-quadruplex/hemin that would further repel the transfer of the negatively charged probe ($Fe(CN)_6^{3-/4-}$). The changes of the current intensity in cyclic voltammetry of different modified electrodes were consistent with the results of EIS (Fig. S8B). The reasons for these changes were similar to that of the EIS results.

Viability of the proposed strategy was further investigated by gel electrophoresis (Fig. S9). A very faint band (lane b) was found for target DNA, while no band was observed in lane a or lane c due to the single stranded structure of the capture probe and bio-bar-coded Pt NPs/G-quadruplex/hemin (Huang et al., 2013). A brighter band with a relatively low mobility (lane d) was detected after hybridizing capture probe with target. When the bio-bar-coded Pt NPs/G-quadruplex/hemin was added to the mixture of capture probe and target, the band from the hybridization of capture probe and target became weaker, and a new band with lower mobility was observed (lane e), indicating the formation of the capture probe/target/bio-bar-coded Pt NPs/G-quadruplex/hemin sandwich structure.

In order to guarantee sensitivity and stability, we investigated the influences of hybridization temperature and incubation time of DNA on the responses of the sensor. It was found that the PEC response of the developed DNA sensor approached its maximum at 37 °C for 1 h (Fig. S10). In addition, we also investigated the effect of the catalytic reaction time between the bio-bar-coded Pt NPs/G-quadruplex/hemin and H_2O_2 on the responses of the developed PEC DNA sensor. The cathodic photocurrent of the developed DNA sensor increased significantly after the addition of 2.0×10^{-4} mol/L H_2O_2 and reached a platform 2 min later (Fig.

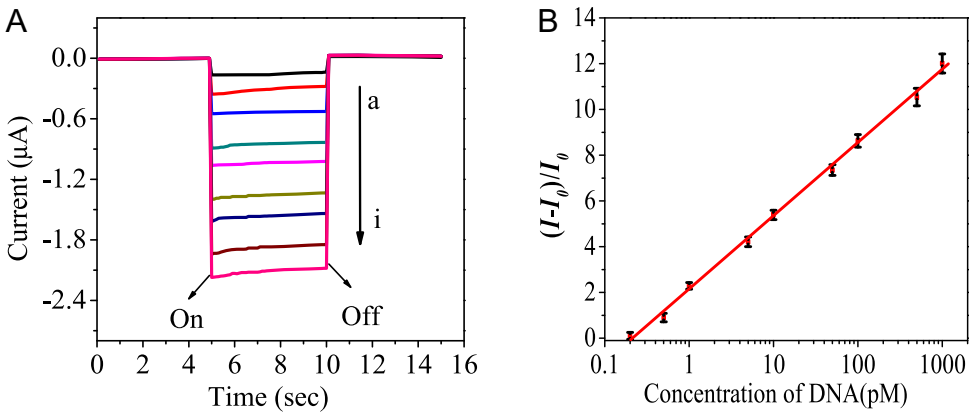

Fig. 4. (A) Photocurrent responses of the ITO/PbS electrode to different concentrations of target DNA, from a to i, the concentration of the target DNA was (pM) 0, 0.5, 1.0, 5.0, 10, 50, 100, 500, 1000, respectively. (B) Plot of photocurrent change $((I-I_0)/I_0)$ of the ITO/PbS electrode vs logarithm C_{DNA}.

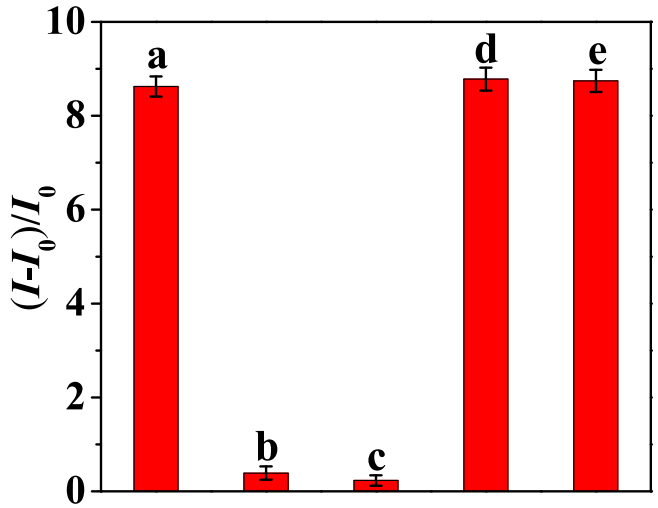

Fig. 5. Photocurrent responses $((I-I_0)/I_0)$ of the detection system to target DNA (a), nonspecific control 1 (b), nonspecific control 2 (c), the mixture of target and nonspecific control 1 (c), and the mixture of target and nonspecific control 2 (d). The concentration of target or noncomplementary DNA was 100 pM.

S11), which was mainly because of the sufficient decomposition of H_2O_2 by the bio-bar-coded Pt NPs/G-quadruplex/hemin complex. The efficient catalytic activity of the bio-bar-code enabled a rapid PEC detection.

Under the optimized experimental conditions, the cathodic photocurrent of the ITO/PbS electrode increased with the increase of the concentration of target DNA (Fig. 4A). A good linear relationship ($R=0.996$) existed between the photocurrent increase ($\Delta I/I_0$, $\Delta I=I-I_0$) and the logarithm of the concentration of target DNA over the range from 0.2 to 1000 pM (Fig. 4B). The detection limit was 0.08 pM. This detection limit was not only much lower than other assays for the detection of target DNA with different measurement protocols such as electrochemistry (Wan et al., 2014; Cui et al., 2014; Dharuman and Hahn, 2008), fluorimetry (Zhu et al., 2014; Sun et al., 2014; Sharon et al., 2010; Zhang et al., 2013), colorimetry (Nie et al., 2014), but also much lower than those PEC detection with different amplification strategies (Golub et al., 2012; Liu et al., 2006, 2008). The detailed comparison for different methods is listed in Table S2.

3.5. Selectivity, stability and reproducibility

The selectivity of the method was tested by replacing the target DNA by non-complementary DNA (nonspecific control 1 and nonspecific control 2). It was found that the photocurrent increases corresponding to nonspecific control 1 and nonspecific control 2 were only 4.5% and 2.7% of the complementary DNA's signal (Fig. 5), indicating the good selectivity of the developed DNA sensor. The addition of non-complementary DNA also hardly affected the PEC response from target DNA. Although CdS or CdTe QDs showed PEC response to oxygen, they also showed response to a variety of electron donors (Wang et al., 2009a, 2009b; An et al., 2010; Schubert et al., 2010; Long et al., 2011; Zhao et al., 2012; Hao et al., 2012). However, it was found that PbS QDs showed no response to 5.0×10^{-5} mol/L ascorbic acid, dopamine, uric acid or cysteine. This also demonstrated the improved selectivity of PbS QDs than CdS or CdTe in PEC biosensing. After a storage time of one week in a refrigerator at 4 °C, no obvious decrease in the photocurrent response to target DNA was observed. After one month, the photocurrent response still retained 92.1% of the initial response value, thereby suggesting acceptable stability of the DNA sensor. Five PEC sensors were prepared independently at the identical experiment conditions, which showed relative standard deviation (RSD) of 2.64%, indicating good reproducibility of the DNA sensor.

4. Conclusions

In conclusion, by coupling the CAT mimetics of the bio-bar-coded Pt NPs/G-quadruplex/hemin for signal amplification, p-type TGA-capped PbS QDs was exploited as a new type of photocathode in PEC DNA sensing for the first time. The enzyme-like activity of the bio-bar-coded Pt NPs/G-quadruplex/hemin even slightly exceeded that of the natural CAT in the decomposition of H_2O_2 to oxygen. This high catalytic activity insured efficient signal amplification. The developed PEC biosensor showed excellent analytical performance for the detection of target DNA with high sensitivity, selectivity, rapid response and good reproducibility. The present method explored the application of PbS QDs-based photocathode in PEC DNA sensors and might be easily extended to other affinity biosensing in photoelectrochemistry.

Acknowledgements

This work was supported by the National Natural Science Foundation of China (Nos. 21275065, 21005031), the Fundamental Research Funds for the Central Universities (JUSRP51314B), the MOE & SAFEA for the 111 Project (B13025).

Appendix A. Supplementary information

Supplementary data associated with this article can be found in the online version at http://dx.doi.org/10.1016/j.bios.2015.02.027.

References

Acharya, H.N., Bose, H.N., 1971. Phys. Status Solidi A 6, K43–K45.
Ammam, M., Fransaer, J., 2011. Sens. Actuators B—Chem. 160, 1063–1069.
An, Y.R., Tang, L.L., Jiang, X.L., Chen, H., Yang, M.C., Jin, L.T., Zhang, S.P., Wang, C.G., Zhang, W., 2010. Chem.—Eur. J 16, 14439–14446.
Beitollahi, H., Mazloum-Ardakani, M., Ganjipour, B., Naeimi, H., 2008. Biosens. Bioelectron. 24, 362–368.
Choudhary, S., Upadhyay, S., Kumar, P., Singh, N., Satsangi, V.R., Shrivastav, Rt, Dass, S., 2012. Int. J. Hydrog. Energy 37, 18713–18730.
Cui, H.F., Cheng, L., Zhang, J., Liu, R.H., Zhang, C., Fan, H., 2014. Biosens. Bioelectron. 56, 124–128.
Deng, M.G., Zhang, D., Zhou, Y.Y., Zhou, X., 2008. J. Am. Chem. Soc. 130, 13095–13102.
Dharuman, V., Hahn, J.H., 2008. Biosens. Bioelectron. 23, 1250–1258.
Fan, J., Yin, J.J., Ning, B., Wu, X.C., Hu, Y., Ferrari, M., Anderson, G.J., Wei, J.Y., Zhao, Y. L., Nie, G.J., 2011. Biomaterials 32, 1611–1618.
Gao, Z., Xu, M., Hou, L., Chen, G., Tang, D., 2013. Anal. Chem. 85, 6945–6952.
Gao, L.Z., Zhuang, J., Nie, L., Zhang, J.B., Zhang, Y., Gu, N., Wang, T.H., Feng, J., Yang, D. L., Perrett, S., Yan, X., 2007. Nat. Nanotechnol. 2, 577–583.
García-Valenzuela, J.A., Baez-Gaxiola, M.R., Sotelo-Lerma, M., 2013. Thin Solid Films 534, 126–131.
Golub, E., Niazov, A., Freeman, R., Zatsepin, M., Willner, I., 2012. J. Phys. Chem. C 116, 13827–13834.
Hao, Q., Wang, P., Ma, X., Su, M., Lei, J., Ju, H., 2012. Electrochem. Commun. 21, 39–41.
Hu, C.C., Nian, J.N., Teng, H., 2008. Sol. Energy Mater. Sol. Cells 92, 1071–1076.
Huang, T., Chen, J., Zhao, S., Shi, M., Chen, Z.F., Liang, H., 2013. Anal. Chem. 85, 4423–4430.
Jankovič, L., Dimos, K., Bujdák, J., Koutselas, I., Madejová, J., Gournis, D., Karakassides, M.A., Komadela, P., 2010. Phys. Chem. Chem. Phys. 12, 14236–14244.
Kang, Q., Liu, S.H., Yang, L.X., Cai, Q.Y., Grimes, C.A., 2011. ACS Appl. Mater. Interfaces 3, 746–749.
Kaya, M., Volkan, M., 2012. Anal. Chem. 84, 7729–7735.
Li, C.L., Liu, K.T., Lin, Y.W., Chang, H.T., 2011. Anal. Chem. 83, 225–230.
Liu, S.L., Li, C., Cheng, J., Zhou, Y.X., 2006. Anal. Chem. 78, 4722–4726.
Long, Y.T., Kong, C., Li, D.W., Li, Y., Chowdhury, S., Tian, H., 2011. Small 7, 1624–1628.
Lu, H., Hu, N., 2006. Electroanalysis 18, 1511–1522.
Lu, W., Jin, Y., Wang, G., Chen, D., Li, J.H., 2008. Biosens. Bioelectron. 23, 1534–1539.
Mazloum-Ardakani, M., Beitollahi, H., Amini, M.K., Mirkhalafc, F., Mirjalili, B., 2011. Biosens. Bioelectron. 26, 2102–2106.
Mazloum-Ardakani, M., Taleata, Z., Khoshrooa, A., Beitollahi, H., Dehghani, H., 2012. Biosens. Bioelectron. 35, 75–81.
Messens, J., Collet, J.F., 2006. Int. J. Biochem. Cell B 38, 1050–1062.
Mu, J.S., Wang, Y., Zhao, M., Zhang, L., 2012. Chem. Commun. 48, 2540–2542.
Nelson, D.P., Kiesow, L.A., 1972. Anal. Biochem. 49, 474–478.
Nie, J., Zhang, D.W., Tie, C., Zhou, Y.L., Zhang, X.X., 2014. Biosens. Bioelectron. 56, 237–242.
Patolsky, F., Katz, E., Willner, I., 2002. Angew. Chem. Int. Ed. 114, 3548–3552.
Perfezou, M., Turner, A., Merkoci, A., 2012. Chem. Soc. Rev. 41, 2606–2622.
Powar, S., Daeneke, T., Ma, M.T., Fu, D.C., Duffy, N.W., Götz, G., Weidelener, M., Mishra, A., Bäuerle, P., Spiccia, L., Bach, U., 2013. Angew. Chem. Int. Ed. 52, 602–605.
Qian, Q., Deng, J.J., Wang, D.L., Yang, L.F., Yu, P., Mao, L.Q., 2012. Anal. Chem. 84, 9579–9584.
Rabani, E., Baer, R., 2010. Chem. Phys. Lett. 496, 227–235.
Roberto, D.L.R., Stevens, M.M., 2012. Nat. Nanotechnol. 7, 821–824.
Sambur, J.B., Novet, T., Parkinson, B.A., 2010. Science 330, 63–66.
Scholes, G.D., Rumbles, G., 2006. Nat. Mater. 5, 683–696.
Schubert, K., Khalid, W., Yue, Z., Parak, W.J., Lisdat, F., 2010. Langmuir 26, 1395–1400.
Seghaier, S., Kamoun, N., Brini, R., Amara, A.B., 2006. Mater. Chem. Phys. 97, 71–80.
Sharon, E., Freeman, R., Willner, I., 2010. Anal. Chem. 82, 7073–7077.
Shi, H., Zhao, G., Liu, M., Zhu, Z., 2011. Electrochem. Commun. 13, 1404–1407.
Shimron, S., Wang, F.A., Orbach, R., Willner, I., 2012. Anal. Chem. 84, 1042–1048.
Sukhovatkin, V., Hinds, S., Brzozowski, L., Sargent, E.H., 2009. Science 324, 1542–1544.
Sun, X.P., Xing, Z.C., Ning, R., Asiri, A.M., Obaid, A.Y., 2014. Analyst 139, 2318–2321.
Travascio, P., Witting, P.K., Mauk, A.G., Sen, D., 2001. J. Am. Chem. Soc. 123, 1337–1348.
Tu, W.W., Wang, W.J., Lei, J.P., Deng, S.Y., Ju, H.X., 2012. Chem. Commun. 48, 6535–6537.
Wan, Y., Wang, P.J., Su, Y., Zhu, X.H., Yang, S.L., Lu, J.X., Gao, J.M., Fan, C.H., Huang, Q., 2014. Biosens. Bioelectron. 55, 231–236.
Wang, G.L., Liu, K.L., Dong, Y.M., Wu, X.M., Li, Z.J., Zhang, C., 2014. Biosens. Bioelectron. 62, 66–72.
Wang, G.L., Xu, J.J., Chen, H.Y., 2009a. Sci. Chin. Ser. B 52, 1789–1800.
Wang, G.L., Yu, P.P., Xu, J.J., Chen, H.Y., 2009b. J. Phys. Chem. C 113, 11142–11148.
Wang, G.L., Xu, J.J., Chen, H.Y., 2010. Nanoscale 2, 1112–1114.
Wang, P.P., Ge, L., Ge, S.G., Yu, J.H., Yan, M., Huang, J.D., 2013. Chem. Commun. 49, 3294–3296.
Wang, X.Y., Zhang, Y.C., Li, T.F., Tian, W.D., Zhang, Q., Cheng, Y.Y., 2013. Langmuir 29, 5262–5270.
Wei, H., Wang, E.K., 2013. Chem. Soc. Rev. 42, 6060–6093.
Xie, J.X., Zhang, X.D., Wang, H., Zheng, H.Z., Huang, Y.M., 2012. TrAC—Trend. Anal. Chem. 39, 114–129.
Yeh, T.F., Chen, S.J., Yeh, C.S., Teng, H., 2013. J. Phys. Chem. C 117, 6516–6524.
Yu, A., Caruso, F., 2003. Anal. Chem. 75, 3031–3037.
Yu, Y.X., Zhang, K.X., Sun, S.Q., 2012. Appl. Surf. Sci. 258, 7181–7187.
Yuan, Y.L., Yuan, R., Chai, Y.Q., Zhuo, Y., Ye, X.Y., Gan, X.X., Bai, L.J., 2012. Chem. Commun. 48, 4621–4623.
Zachariou, M., Hearn, M.T.W., 2000. J. Chromatogr. A 890, 95–116.
Zhang, L.B., Zhu, J.B., Guo, S.J., Li, T., Li, J., Wang, E.K., 2013. J. Am. Chem. Soc. 135, 2403–2406.
Zhang, S., Shao, Y.Y., Yin, G.P., Lin, Y.H., 2009. J. Mater. Chem. 19, 7995–8001.
Zhao, W.W., Xu, J.J., Chen, H.Y., 2014. Chem. Rev. 114, 7421–7441.
Zhao, X.M., Zhou, S.W., Shen, Q.M., Jiang, L.P., Zhu, J.J., 2012. Analyst 137, 3697–3703.
Zhu, H.W., Wang, G.D., Xie, D.L., Cai, B., Liu, Y.M., Zhao, X.Z., 2014. Biomed. Microdevices 16, 479–485.